The Research on Controlling Groundwater Pollution Caused by In-Situ Leaching Uranium: A Case Study in Bayan-Uul Area, Northern China

Haibo Li , Zhonghua Tang , Dongjin Xiang *

Posted Date: 31 October 2023

doi: 10.20944/preprints202310.1980.v1

Keywords: Uranium; In-situ leaching; Reactive transport model; Capture zone; Streamline; pollution control

Article

The Research on Controlling Groundwater Pollution Caused by In-Situ Leaching Uranium: A Case Study in Bayan-Uul Area, Northern China

Haibo Li [1], Zhonghua Tang [1] and Dongjin Xiang [2,*]

[1] School of Environmental Studies, China University of Geosciences, Wuhan, Hubei, 430074; China; zhhtang@cug.edu.cn; lhb0163a@163.com

[2] School of Mathematics and Physics, China University of Geosciences, Wuhan, Hubei,430074; China

* Correspondence: xiangdongjin@cug.edu.cn

Abstract: Acid in-situ leaching (ISL) is a common approach to the recovery of uranium in the subsurface. As some toxic and harmful substances might be produced by the chemical reactions among the injected sulphuric acid, the groundwater, and the porous media during leaching processes, the pollution control of the mining plan for ISL is important. In this study, a three-dimensional reactive transport modeling (3DRTM) was applied to decide the pollution control mining plan, considering the partial penetration through wellbore in confined aquifer and complex chemical reactions between main minerals. Based on the 3DRTM, different pumping ratio and non-uniform injection schemes were compared. The results show that the preferential pollution control mining plan is non-uniform injection ratio equal 0.1. By analyzing the characteristics of water table and streamline, it is concluded that the scheme has a strong hydraulic capture effect. In this scheme, the concentration of UO_2^{2+}, H^+, SO_4^{2-} obtained by 3DRTM is lower. The inner well injection rate is 194.09 m^3/d, the outer well injection rate is 158.89 m^3/d, and the pumping rate is 264.00 m^3/d. A reasonable suggestion is to adopt non-uniform injection mining mode in ISL.

Keywords: uranium; in-situ leaching; Reactive transport model; Capture zone; Streamline; pollution control

1. Introduction

ISL (in-situ leaching) is an important technique in sandstone uranium deposits with high permeability [1]. Due to the complex chemical composition in the lixiviant of the ISL project, the groundwater will be polluted if it is not properly controlled [2-5]. There are many groundwater environmental challenges caused by ISL [6]. Some radioactive elements and heavy metals can enter groundwater and cause groundwater pollution [7]. Developing effective technology for ISL is imperative. Therefore, effective control of groundwater pollution caused by in-situ leaching of uranium has always been a widespread concern, and many scholars and engineering technicians have conducted extensive research on this issue.

Many researchers use numerical methods to design optimal recovery plans and control the pollution of acid in-situ leaching uranium on groundwater. Based on the actual production data of a sandstone uranium mine, a unit flow model of the ISL uranium mining area using the groundwater modeling system (GMS) is established [8]. And then proposes a scheme and establishes a hydrodynamic model of the leaching range under eight different pumping and injection conditions by using the GMS [9]. However, in these researches, the hydrogeochemical reaction is not sufficiently considered.

Although some reactive transport models (RTM) have been built to predict fluid flow and geochemical reactions in reservoirs [10,11]. The minerals considered are uranium minerals, iron oxides, and carbonate minerals, but not consider compositions such as K-feldspar, albite, and clay minerals, which exist in large quantities in the sand-stone stratum [12-15]. The three dimensional reactive transport models(3DRTM) of ISL considering the partial penetration through wellbore

 doi:10.20944/preprints202310.1980.v1

structure and the complex chemical reactions has not been built. It is difficult to directly describe the real situation of the field. To summarize, the current research is insufficient for numerical simulation about the 3DRTM with multi-mineral components in actual sites, which also makes it difficult to consider various chemical reactions in pollution control problems based on models. Therefore, it is necessary to synthesize the existing studies and characterize the particularities of ISL based on these studies.

To effectively control the migration of pollutants in groundwater, scholars have put forward a series of measures [16]. Among them, hydraulic capture is a simple, effective, and widely used pollution control method, which is used to control the oil pollutants diffusion [17], and optimize the number, location, and structure of pumping wells [18-21]. With the development of numerical simulation technology, hydraulic capture methods were adopted to control the effect of pollutant migration combined with MODFLOW and MT3D [22]. These methods are especially suitable for well-group production scenarios. However, during the ISL process, hydrogeochemical reactions have a great influence. These studies do not consider chemical reactions adequately so that the calculated errors exist in using MODFLOW or MT3DMS. Therefore, a more realistic approach is to substitute the pollution control scheme calculated from the capture zone into RTM for comparative calculation. For ISL, this analysis combined with RTM applied to the actual field is lacking.

Bayan-Uul mining area is a sandstone uranium deposit. The hydrogeological data of this mining area is comprehensive, with relatively complete historical data and monitoring data. For this area, the influence of different injection flow rates, injection well distances, flow velocity fields, and leaching ranges has been studied through established hydrodynamic model by Visual Modflow [23, 24]. However, in these models, hydrogeochemical processes are not considered. PHT3D has been used to investigate the effects of mineral composition, reaction kinetics, pumping flow rate, and pumping well spacing on pitchblende leaching and uranium migration in ore-bearing aquifers [25]. Nevertheless, the model establishes one and two-dimensional models respectively, and only considers the calcite, pyrite, hematite, and uranium minerals.

In this study, a three-dimensional reactive transport model (3DRTM) has been built by TOUGHREACT. The model considered the partial penetration through wellbore structure, abundant minerals and water-rock interactions. The 3DRTM can describe the pollution plume more accurately. Then several schemes of different pumping ratios and non-uniform injection ratio are simulated using calibrated 3DRTM. By comparing the simulation results based on the hydraulic capture zone, streamline, and 3DRTM, a pollution scheme considering the lower concentration of UO_2^{2+}, H^+, and SO_4^{2-} at the observation well was obtained. This work provided some reference for the pollution control of in-situ uranium leaching.

2. Conceptual model and mathematical model

2.1. Geological settings of the study area

(1) Geological settings

Bayan-Uul mining area is located in the north of the Inner Mongolia Autonomous Region. It is about 30km to the north of Sonid Zuoqi city. Figure 1 is the location map and the distribution of boreholes in the mining area.

Preprints (www.preprints.org) | NOT PEER-REVIEWED | Posted: 31 October 2023 doi:10.20944/preprints202310.1980.v1

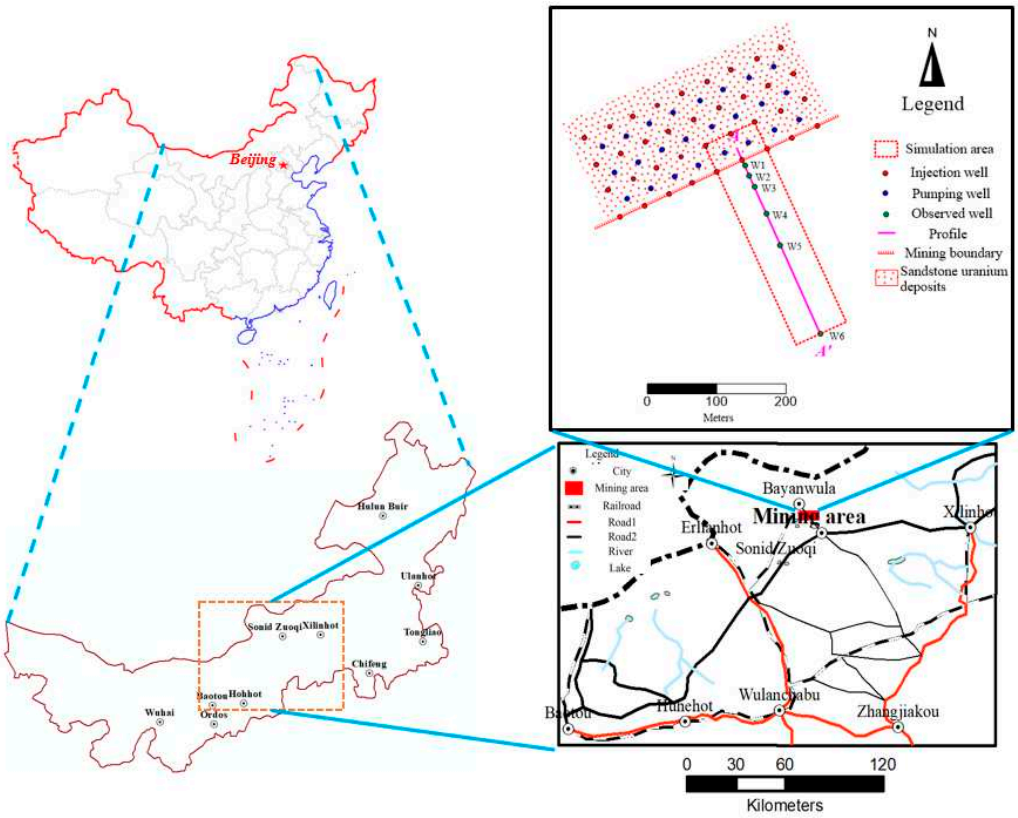

Figure 1. Location map of the mining area with borehole geographical details.

Figure 2 is a hydrogeological section of the study area. It can be seen from the figure that the main confined aquifer is located in the upper section of the Saihan Formation (K_1s^2), and the aquifer is horizontal. This aquifer is composed of sandstone and sandy conglomerate and has a good water yield and permeability. The thickness of this aquifer is about 60 meters.

The Irdimanha Formation (E_2y) is distributed at the top of K_1s^2. It mainly consists of a group of rivers and flood sedimentary sandstone, sand gravel, mud gravel, sand, mud, and rocks. The thickness is about 50m. This layer is the water barrier roof of aquifer K_1s^2. The lower section of the Saihan Formation (K_1s^1) is composed of mudstone and silty mudstone mixed with lignite mined in the lake and marsh. The thickness of borehole exposure is generally 5 meters to 60 meters, forming a stable water-resisting floor of the aquifer K_1s^2. The stratigraphic structure is relatively neat. The water head is very gentle, which is taken as 941 meters through actual measurement.

Preprints (www.preprints.org) | NOT PEER-REVIEWED | Posted: 31 October 2023 doi:10.20944/preprints202310.1980.v1

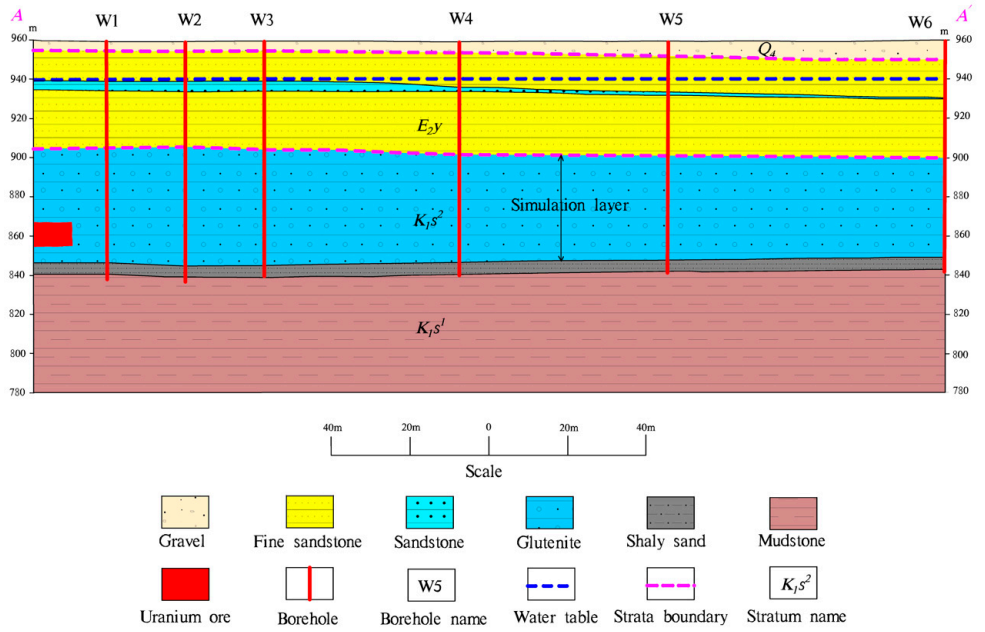

Figure 2. Hydrogeological section of the study area.

(2) Conceptual model

In this study, the scope of the simulated region includes two pumping units. To study the influence of ISL on the outside of the mining area, the simulation area also includes areas outside the pumping unit, which are up to 300 meters away from the pumping unit. (Figure 3)

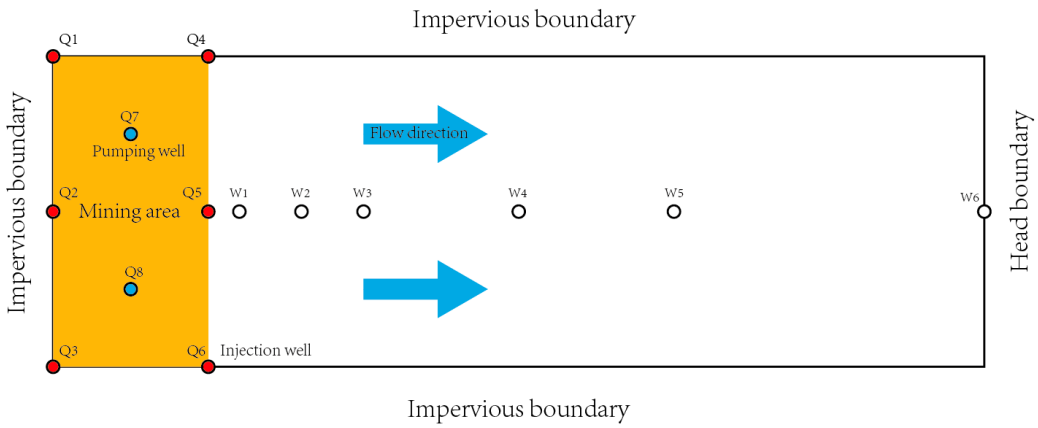

Figure 3. Conceptual model of reactive transport.

2.2. Governing equations

The governing equation involved in the model is as follows [26]:

(1) Water flow equation

The equation can be established from the conservation of mass:

$$\frac{\partial M_\kappa}{\partial t} = -\nabla F_\kappa + q_\kappa \tag{1}$$

For water phase:

$$F_w = x_{wl}\rho_l\overrightarrow{u_l} + x_{wg}\rho_g\overrightarrow{u_g},\ q_w = q_{wl} + q_{wg} \tag{2}$$

The mass flux of the multi-phase is according to Darcy's law:

Preprints (www.preprints.org) | NOT PEER-REVIEWED | Posted: 31 October 2023 doi:10.20944/preprints202310.1980.v1

$$\overrightarrow{u_\beta} = -k\frac{k_{r\beta}}{\mu_\beta}\left(\nabla P_\beta - \rho_\beta \vec{g}\right) \tag{3}$$

Combine with the mass conservation equation, the reactive transport model can be expressed as:

$$\frac{d\left(\varphi S_l c_{jl}\right)}{dt} = -\nabla\left(c_{jl}\overrightarrow{u_l} - \tau\varphi S_l D_l \nabla c_{jl}\right) + \sum_{i=1}^{N} \nu_{jn} r_n \tag{4}$$

Table 1. The mathematical model parameters.

symbol	meaning	symbol	meaning
$\boldsymbol{M_\kappa}$	The total mass of matter $\boldsymbol{\kappa}$	$\boldsymbol{S}$	saturation
$\boldsymbol{t}$	Time	$\boldsymbol{\varphi}$	porosity
$\boldsymbol{F_\kappa}$	Flow rate of matter $\boldsymbol{\kappa}$	$\boldsymbol{k}$	Absolute permeability
$\boldsymbol{q_\kappa}$	Source and sink of matter $\boldsymbol{\kappa}$	$\boldsymbol{k_r}$	Relative permeability
$\boldsymbol{w}$	water	$\boldsymbol{\mu}$	viscosity
$\boldsymbol{c}$	concentration	$\boldsymbol{l}$	Liquid phase
$\boldsymbol{x}$	Mass fraction	$\boldsymbol{g}$	Gas phase
$\boldsymbol{\rho}$	density	$\boldsymbol{D}$	Dispersion
$\boldsymbol{u}$	Velocity of flow	$\boldsymbol{r}$	reaction rate
$\boldsymbol{\nu}$	stoichiometric number	$\boldsymbol{j}$	species $\boldsymbol{j}$
$\boldsymbol{P}$	pressure	$\boldsymbol{n}$	Reaction $\boldsymbol{n}$

(2) Chemical reaction mathematical models

The main chemical reaction mathematical models in the simulation include equilibrium minerals and kinetic minerals. The equilibrium mineral model is:

$$\Omega_m = K_m^{-1}\prod_{j=1}^{N_c} c_j^{\nu_{mj}}\gamma_j^{\nu_{mj}} \tag{5}$$

Where K_m is the equilibrium constant.

The kinetic mineral model is:

$$r_n = \pm k_n A_n\left|1 - \Omega_n^\theta\right|^\eta \tag{6}$$

Where A_n is the specific surface area of the mineral; k_n is the nth parallel mineral precipitation or dissolution reaction rate constant that depends on temperature;

Based on the Arrhenius equation, the correlation between k_n and temperature can be written as:

$$k_n = k_{25}^{nu} exp\left[-\frac{E_a^{nu}}{R}\left(\frac{1}{T} - \frac{1}{298.15}\right)\right] + \sum_i \left\{k_{25}^i exp\left[-\frac{E_a^i}{R}\left(\frac{1}{T} - \frac{1}{298.15}\right)\right]\right\}\prod_j a_{ij}^{n_{ij}} \tag{7}$$

where $\prod_j a_{ij}^{n_{ij}}$ describes the effect of specific ion activity on the i th parallel mineral precipitation and dissolution reaction;

(3) Models of mineral dissolution or precipitation

Based on the geological condition, the uranium mineral is UO_2. The minerals include Quartz, K-feldspar, Na-feldspar, oligoclase, Na-smectite, Ca-smectite, illite, kaolinite, gypsum and anhydrite, hematite, muscovite, dolomite, siderite, and ankerite. These minerals are also considered in the model. Here we've listed some chemical reactions.

$$2NaAlSi_3O_8 + H_2SO_4 + 9H2O \rightarrow 2Na^+ + SO_4^{2-} + Al_2Si_2O_5(OH)_4 + 4H_4SiO_4 \tag{8}$$

$$2KAlSi_3O_8 + H_2SO_4 + 9H_2O \rightarrow 2K^+ + SO_4^{2-} + Al_2Si_2O_5(OH)_4 + 4H_4SiO_4 \tag{9}$$

Preprints (www.preprints.org) | NOT PEER-REVIEWED | Posted: 31 October 2023 doi:10.20944/preprints202310.1980.v1

$$2K_{0.5}Mg_{0.25}Al_{2.3}Si_{3.5}O_{10}(OH)_2 + \frac{11}{10}H_2SO_4 + \frac{63}{20}H_2O \rightarrow \frac{1}{2}K^+ + Mg^{2+} + SO_4^{2-} + Al_2Si_2O_5(OH)_4 + \frac{6}{5}H_4SiO_4 \quad (10)$$

$$CaCO_3 + H_2SO_4 \rightarrow CaSO_4 + CO_2 + H_2O \quad (11)$$

$$CaMg(CO_3)_2 + 2H_2SO_4 \rightarrow CaSO_4 + Mg^{2+} + SO_4^{2-} + 2CO_2 + 2H_2O \quad (12)$$

$$H_4SiO_4 \rightarrow SiO_2 + 2H_2O \quad (13)$$

$$Fe_2O_3 + 3H_2SO_4 \rightarrow 2Fe^{3+} + 3SO_4^{2-} + 3H_2O \quad (14)$$

(4) Relative permeability and capillary pressure calculation model

The calculation model of relative permeability and capillary pressure adopts the Van Genuchten-Mualem model.

2.3. Initial conditions and boundary conditions

(1) Initial conditions

Based on field investigation results, the initial temperature of the aquifer has been set as 9℃, and the initial head is 941 meters. In order to obtain the initial concentration of each ion in the aquifer, we conducted a field sampling analysis. The initial concentration of ions is listed in Table 2. The resulting individual sample analysis results are substituted into the model as the initial concentration. The initial minerals considered in this study include Quartz, K-feldspar, Na-feldspar, oligoclase, Na-smectite, Ca-smectite, illite, kaolinite, uranium, hematite, calcite. The initial mineral composition of the ore layer can be see in Table 3.

Table 2. Initial concentration.

Index	Concentration
Na(mg/L)	495
K(mg/L)	8.46
Ca(mg/L)	76.6
Mg(mg/L)	55.2
SO_4^{2-}(mg/L)	407
Cl^-(mg/L)	410
HCO_3^-(mg/L)	1110
Fe(mg/L)	0.747
U(μg/L)	30.1

Table 3. Initial mineral composition.

name	Chemical formula	Initial mineral volume fraction of ore body	Initial mineral volume fraction of surrounding rock
Quartz	SiO_2	0.48686	0.48686
K-feldspar	$KAlSi_3O_8$	0.21550	0.21550
Oligoclase	$CaNa_4Al_6Si_{14}O_{40}$	0.01134	0.01134
Na-smectite	$Ca_{0.145}Mg_{0.26}Al_{1.77}Si_{3.97}O_{10}(OH)_2$	0.08391	0.08391
Ca-smectite	$Na_{0.29}Mg_{0.26}Al_{1.77}Si_{3.97}O_{10}(OH)_2$	0.02597	0.02597

Preprints (www.preprints.org) | NOT PEER-REVIEWED | Posted: 31 October 2023 doi:10.20944/preprints202310.1980.v1

Illite	$K_{0.6}Mg_{0.25}Al_{1.8}(Al_{0.5}Si_{3.5}O_{10})(OH)_2$	0.02137	0.02137
Kaolinite	$Al_2Si_2O_5(OH)_2$	0.01520	0.01520
Uraninite	UO_2	0.01143	0.00000
Hematite	Fe_2O_3	0.01880	0.01880
Calcite	$CaCO_3$	0.03320	0.01140

(2) Boundary conditions

In this study, through field investigation, we found that the change of water head is weakly affected by mining at the position 200 meters to 300 meters away from the mining area. Therefore, according to the water head value of the observation well 300 meters away from the mining area, the boundary water head of the model is set to 941 meters.

3. Numerical model

3.1. Software

Based on the mathematical model, the simulator TOUGHREACT is used to build the numerical model. In this study, a reactive transport of mining area mining has been built. A variety of mineral components and water-rock interactions are involved in the model. The simulator is TOUGHREACT. TOUGHREACT [27] was developed by introducing reactive geochemistry into the framework of TOUGH2V2 [28]. TOUGHREACT has been applied to simulate a wide range of subsurface hydrological and biogeochemical environments. For example, geothermal systems [29], nuclear waste repositories [30], geologic carbon sequestration [31, 32], and environmental remediation [33, 34].

3.2. Mesh setting

According to the scope of the study area, we use arbitrary polygonal mesh in the horizontal direction to produce the mesh. In the plumb direction, rectangular mesh is used to produce mesh.

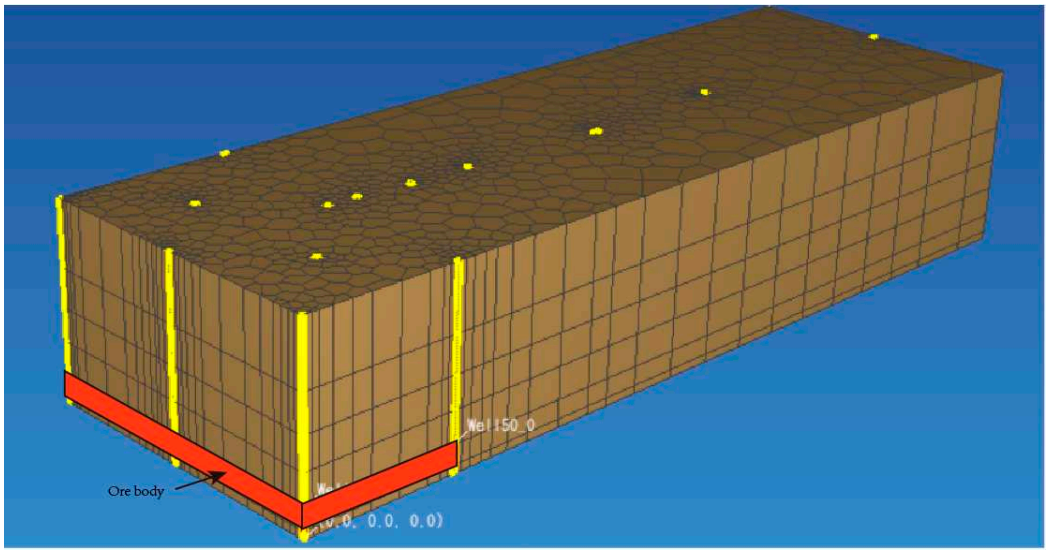

Figure 4. 3D structure diagram of mesh.

3.3. Parameters

Preprints (www.preprints.org) | NOT PEER-REVIEWED | Posted: 31 October 2023 doi:10.20944/preprints202310.1980.v1

Based on the regional geological report, the spatial location information of the parameters, and the initial parameter setting of the model for the mineral components information have been confirmed (Table 4). The chemical reaction parameters please shown in Table 5.

Table 4. The aquifer parameters.

Parameters	Value
Aquifer thickness(m)	60
Rock grain density(kg/m^3)	2600
Porosity	0.085
K: absolute permeability(m^2)	3×10^{-6}
Temperature(℃)	9
Rock grain specific heat(J/(Kg•℃))	920
Formation heat conductivity(W/(m•℃))	2.51
Pressure(MPa)	0.1

Table 5. The mineral reaction kinetic parameters used in the model.

Minerals	Chemical formula	Surface area(cm2/g)	Parameters for kinetic rate law							
			Neutral mechanism		Acid mechanism			Base mechanism		
			k_{25}(mol/m^2/s)	E_a (KJ/mol)	k_{25}(mol/m^2/s)	E_a (KJ/mol)	N (H^+)	k_{25}(mol/m^2/s)	E_a (KJ/mol)	n(OH^-)
Calcite	$CaCO_3$	9.8	Equilibrium							
Anhydrite	$CaSO_4$	9.8	Equilibrium							
Quartz	SiO_2	9.8	1.023×10^{-14}	87.7						
Illite	$K_{0.6}Mg_{0.25}Al_{1.8}(Al_{0.5}Si_{3.5}O_{10})(OH)_2$	151.6	1.660×10^{-13}	35.0	1.047×10^{-11}	23.6	0.34	3.020×10^{-17}	58.9	-0.4
K-feldspar	$KAlSi_3O_8$	9.8	3.890×10^{-13}	38.0	8.710×10^{-11}	51.7	0.5	6.310×10^{-22}	94.1	-0.823
Chlorite	$Mg_{2.5}Fe_{2.5}Al_2Si_3O_{10}(OH)_8$	20.0	3.020×10^{-13}	88.0	7.762×10^{-12}	88.0	0.50			
Na-smectite	$Na_{0.29}Mg_{0.26}Al_{1.77}Si_{3.97}O_{10}(OH)_2$	151.6	1.660×10^{-13}	35.0	1.047×10^{-11}	23.6	0.34	3.020×10^{-17}	58.9	-0.4
Kaolinite	$Al_2Si_2O_5(OH)_4$	23.0	6.918×10^{-14}	22.2	4.898×10^{-12}	65.9	0.777	8.913×10^{-18}	17.9	-0.472
Ca-smectite	$Ca_{0.145}Mg_{0.26}Al_{1.77}Si_{3.97}O_{10}(OH)_2$	151.6	1.660×10^{-13}	35.0	1.047×10^{-11}	23.6	0.34	3.020×10^{-17}	58.9	-0.4
Gypsum	$CaSO_4$	9.8	1.6218e-07							
Pyrite	FeS_2	12.9	2.52×10^{-12}	62.76						
Oligoclase	$CaNa_4Al_{1.77}Si_{3.97}O_{10}(OH)_2$	10.0	1.4454e-13	69.80						
Hematite	Fe_2O_3	12.9	2.512×10^{-15}	66.2	4.0738×10^{-10}	66.2	1			
Muscovite	$KAl_2(AlSi_3O_{10})(OH)_2$	152.0	3.0200×10^{-13}	88.0	7.7624×10^{-12}	88.0	0.5	3.0200×10^{-13}		
Siderite	$FeCO_3$	10.0	1.26×10^{-9}	62.76	6.46×10^{-4}	36.1	0.5			
Dolomite	$CaMg(CO_3)_2$	12.9	2.52×10^{-12}	62.76	2.34×10^{-7}	43.54	1			
Ankerite	$CaMg_{0.3}Fe_{0.7}(CO_3)_2$	9.8	1.26×10^{-9}	62.76	6.46×10^{-4}	36.1	0.5			
Magnesite	$MgCO_3$	10.0	4.5709×10^{-10}	23.50	4.1687×10^{-07}	14.4	1			

3.4. Sources and sinks

Preprints (www.preprints.org) | NOT PEER-REVIEWED | Posted: 31 October 2023 doi:10.20944/preprints202310.1980.v1

We investigated the production data of the mine. According to the survey results, the flow rate of the injection well is 176m³/d, and the flow rate of the pumping well is 264m³/d. The ion concentration of the injection well is also obtained from the field sampling analysis. The sulfuric acid concentration of the injection well is 0.1866 mol/kg.

3.5. Model accuracy and verification

The calibrated accuracy of the concentration field uses the linear correlation coefficient to measure. The correlation coefficients of the three wells ranged from 0.9433 to 0.9990. The simulation accuracy of this study is above 90%. The calibrated accuracy of the concentration field uses the linear correlation coefficient to measure. The expression of the linear correlation coefficient is as follows [35]:

$$r = \frac{\sum_{i=1}^{n}(C_i - \overline{C_i})(b_i - \overline{b_i})}{\sqrt{\sum_{i=1}^{n}(C_i - \overline{C_i})^2}\sqrt{\sum_{i=1}^{n}(b_i - \overline{b_i})^2}} \quad (15)$$

Where, C_i is the simulated concentration, and $\overline{C_i}$ is the mean value of the simulated value; b_i Observed concentration, $\overline{b_i}$ is the mean value of the observed value. Near the simulation area, there are three typical observation holes: W_1, W_2, and W_3. Three observation holes were sampled respectively. The pH value is for the field test, and SO_4^{2-} was sent to the mining area laboratory for analysis and test.

Figure 8, figure 9, and figure 10 show the calibrate points of each test index concentration of each observation well. From the figures, it can be seen that the simulated values of most points are similar to the observed values. The variety trend of the simulated values is consistent with the observed values, indicating that the model can reflect the actual mining and can be used to predict the ISL.

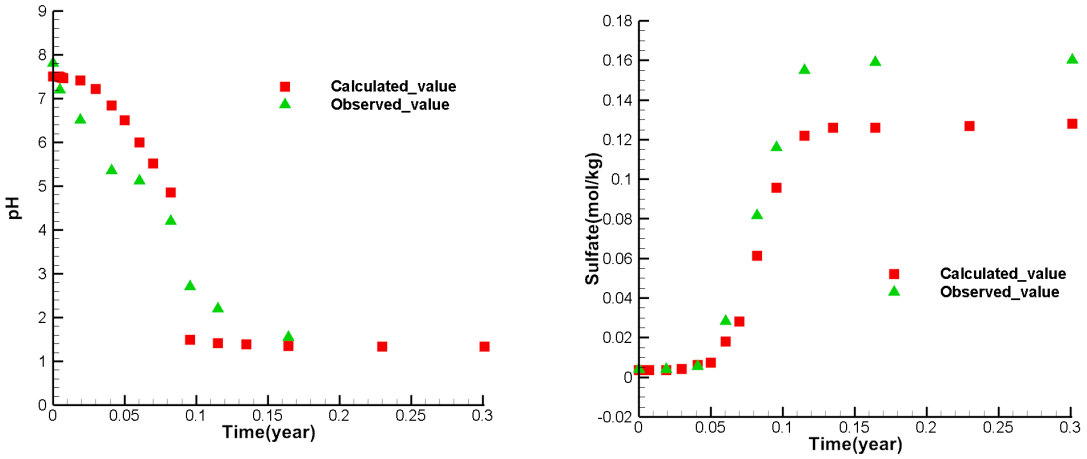

Figure 5. Comparison between observed and simulated values of at the observation well W_1.

Preprints (www.preprints.org) | NOT PEER-REVIEWED | Posted: 31 October 2023 doi:10.20944/preprints202310.1980.v1

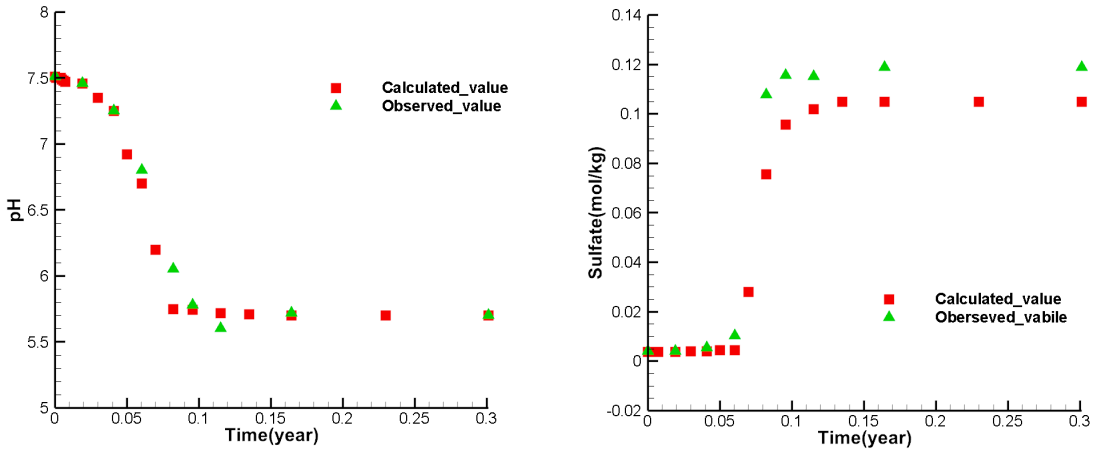

Figure 6. Comparison between observed and simulated values of at the observation well W_2.

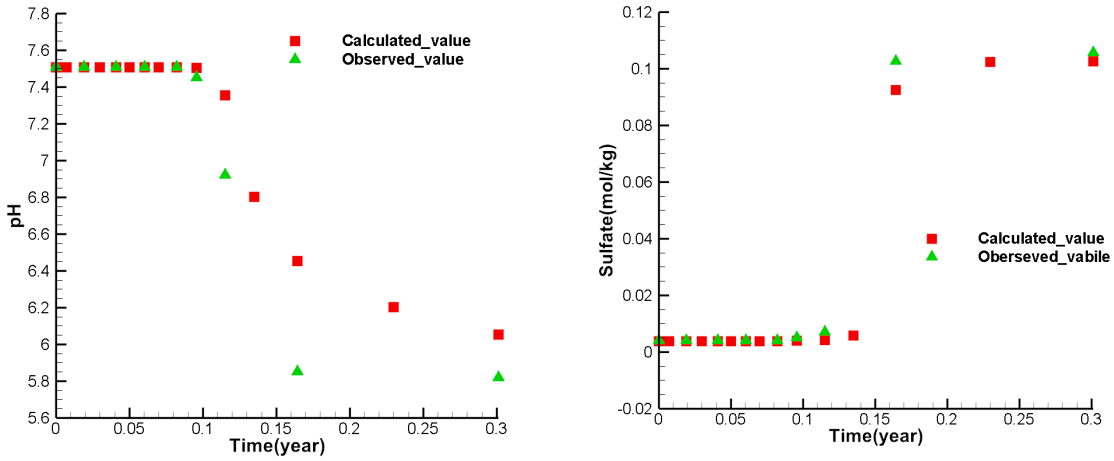

Figure 7. Comparison between calculated values and observed values at the observation well W_3.

4. Influence of in-site-leaching of uranium on groundwater quality

It is important to consider the pumping rate and injection rate when it comes to in-situ leaching (ISL). These rates should be sufficient to meet mining requirements but not so large as to cause pollution. Therefore, it's crucial to find the optimal pumping ratio and non-uniform injection ratio. This study utilized a range of scenarios based on the 3DRTM. The 3DRTM accounted for water-rock interactions, resulting in more accurate and reliable results. The numerical simulation method was used to calculate the groundwater dynamic and hydrogeochemical fields in each scenario. A comparative analysis of the water table contour, streamline, and concentration breakthrough curve at W_1 was conducted to determine the best mining scheme for pollution control.

4.1. Cases setting

Two factors were considered in this study, one is the pumping ratio and the other is the non-uniform injection ratio. These two parameters have a significant influence on in-situ uranium leaching by controlling well flux and leaching fluid composition and are easy to realize in actual production.

(1) Pumping ratio

For the pumping and injection rate, there is a pumping ratio to describe:

Preprints (www.preprints.org) | NOT PEER-REVIEWED | Posted: 31 October 2023 doi:10.20944/preprints202310.1980.v1

$$pumping\ ratio = \frac{(Q_7 + Q_8) - (Q_1 + Q_2 + Q_3 + Q_4 + Q_5 + Q_6)}{(Q_1 + Q_2 + Q_3 + Q_4 + Q_5 + Q_6)} \quad (16)$$

According to the characteristics of actual production, we set $Q_1 = Q_2 = Q_3 = Q_4 = Q_5 = Q_6$, $Q_7 = Q_8$.

Where Q_1, Q_2, and Q_3 as the flow rate of inner injection wells, and define Q_4, Q_5, and Q_6 as the flow rate of outer injection wells. Q_7, Q_8 as the flow rate of pumping wells. The position of them has been given in Figure 3.

(2) Non-uniform injection ratio

The non-uniform injection ratio has been described by:

$$non - uniform\ injection\ ratio = \frac{(Q_1 + Q_2 + Q_3) - (Q_4 + Q_5 + Q_6)}{(Q_4 + Q_5 + Q_6)} \quad (17)$$

According to the characteristics of actual production, we set $Q_1 = Q_2 = Q_3, Q_4 = Q_5 = Q_6, Q_7 = Q_8$.

4.2. Simulation schemes design and the principle of pollution control

(1) Simulation schemes design

Due to the analysis the impact of pumping ratio and non-uniform injection ratio, five schemes have been designed for simulation (scheme 1 to scheme 5). The water level contours and the streamlines are extracted from these models. The contour map of the water level is the fifth layer grid representing the production zone. The profile of the streamlines has been generated at the central axis. After these numerical simulations, the uranium concentration, pH value, and sulfate radical concentration at the observation site W_1 were selected for comparative analysis. Table 4 displays the simulation schemes.

Table 4. The simulation schemes.

	Schemes(Simulation time=1 year)				
	1	**2**	**3**	**4**	**5**
Pumping ratio	0	0.01	0.02	0	0
Non-uniform injection ratio	0	0	0	0.05	0.1
Inner injection rate(m^3/d)	176.00	174.24	172.48	184.82	194.09
Outer injection rate(m^3/d)	176.00	174.24	172.48	167.18	158.89
Pumping rate(m^3/d)	264.00	265.76	267.52	264.00	264.00

(2)The principle of determining the pollution control

After determining the above scheme simulation, the better pollution control scheme selection principle of this study is as follows.

(a) Principle of pollution control based on water level

Based on the numerical simulation results of several schemes, the water table map of the mine layer is extracted respectively. If a scheme can have a higher water head distribution outside the mining area than inside, we believe that this scheme is more optimal.

(b) Principle of pollution control based on streamline

The streamline of the vertical section in Q_2-Q_5-W_1-W_2-W_3-W_4-W_5 is analyzed by comparison. The position of Q_2-Q_5-W_1-W_2-W_3-W_4-W_5 is shown in Fig.3. If the characteristics of the streamline back to the mining area are more obvious, this scheme is the best scheme.

(c) Comparison of concentrations at the observation well.

The concentration simulation value of the W_1 observation well, which is most significantly affected by the mining area, is selected for comparison. The lower the concentration, the more optimal solution we consider.

(3) Sensitivity analysis

Preprints (www.preprints.org) | NOT PEER-REVIEWED | Posted: 31 October 2023 doi:10.20944/preprints202310.1980.v1

Through sensitivity analysis, the parameter with the most significant influence is obtained, which is the priority control parameter. Sensitivity coefficient means how much the dependent variable factor is affected by an independent variable factor. The calculation method is a partial differentiation of the dependent variable concerning the independent variable:

$$S_{ij} = \frac{\partial y_i}{\partial x_j} \tag{18}$$

Where, S_{ij} is the sensitivity coefficient of the ith dependent variable to the jth independent variable. In this study, the difference quotient is used instead of the derivative, and the sensitivity coefficient is calculated by the difference quotient.

$$S_{ij} = \frac{y_i(x_j + \Delta x_j) - y_i(x_j)}{\Delta x_j} \tag{19}$$

where y_i represents the concentration value of the ith index, x_j represents the jth dependent variable, Δx_j represents the increment of the jth dependent variable. In this study, y_i was the concentration when the penetration curve was stable.

5. Results and discussion

5.1. The variation of uranium ore,UO_2^{2+} ,SO_4^{2-},H^+ for base scheme(scheme 1)

(1) Variation of uranium ore content and migration of uranium

When the acid solution is injected into the aquifer, the uranium minerals dissolve in the groundwater, which is the main mechanism of in-situ leaching. In Figure 8 a, the blue area is the uranium dissolution zone, and the red area is the uranium precipitation zone. The maximum volume fraction of a uranium increment may exceed 0.006%, but cannot exceed 0.008%. Uranium ore volume fraction can be reduced by more than 0.01%. The results show that the uranium ore is mainly dissolved. According to the simulation results, the uranium ore is mainly dissolved near the water injection well, which is the main source of uranium in the mining area. Near the injection well, the volume fraction of uranium is reduced to 0.01%. Near pumping wells, the volume fraction of uranium can be increased to 0.006%. This is because of the groundwater flows, the acid in the leaching solution is gradually consumed, which will cause the pH value to be decreased so that the previously dissolved uranium will be precipitated again. Outside the mine area, there is no uranium in the aquifer.

From the distribution of uranium concentration, the uranium concentration near the pumping well is higher. The highest concentration of UO_2^{2+} occurs between injection wells and pumping wells. The maximum concentration of UO_2^{2+} can exceed 0.004 mol/kg. (Figure 8 b)

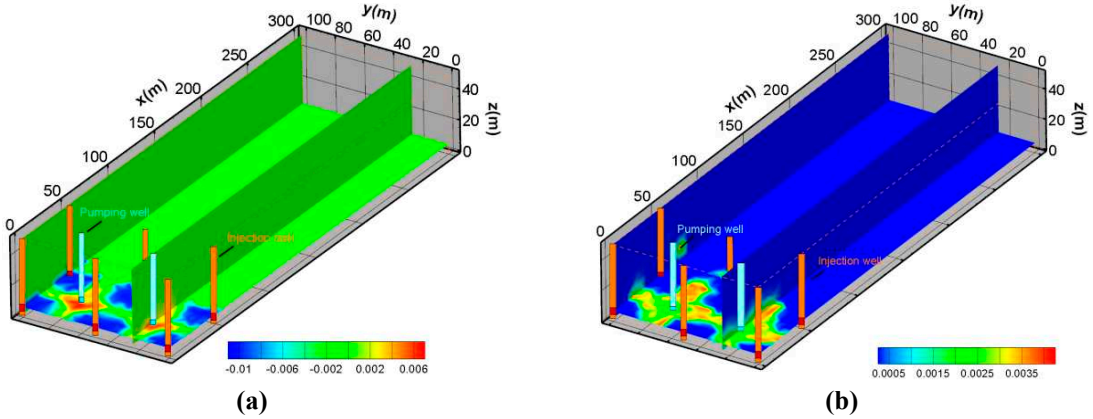

(a) **(b)**

Figure 8. **(a)** Spatial distribution of volume fraction variation of uranium ore body, **(b)** the distribution of the concentration of UO_2^{2+}.

(2) SO_4^{2-} Spatial distribution characteristics

Preprints (www.preprints.org) | NOT PEER-REVIEWED | Posted: 31 October 2023 doi:10.20944/preprints202310.1980.v1

In the acid-leaching process, the amount of sulfuric acid is large. The concentration of SO_4^{2-} is a key indicator that needs to be described. In this simulation, the concentration of SO_4^{2-} is relatively high, with the highest concentration exceeding 0.13mol/Kg. The migration distance can be more than 150m. This is mainly because SO_4^{2-} is a large amount of injected ions in mining areas, and its consumption is limited. Although some SO_4^{2-} interacts with minerals, there is still a large amount of redundancy due to the large amount of injection. The concentration spatial distribution of SO_4^{2-} is shown in Figure 9.

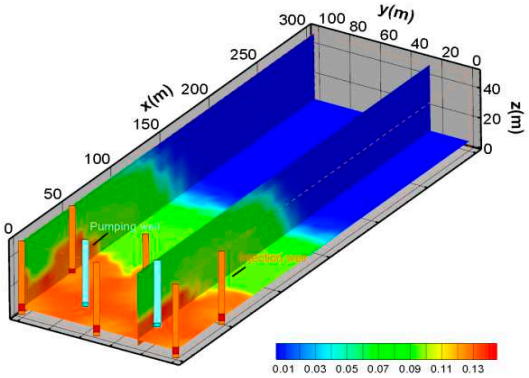

Figure 9. The concentration spatial distribution of SO_4^{2-}.

(3) H^+ spatial distribution characteristics

An important factor affecting ground leaching is H^+ concentration. Figure 10 shows the change in pH after one year of mining. At the inside of mine, the pH value is relatively low. The pH value increases gradually with the distance from the mining area. Figure 10 also shows that if the lower pH value range is extended to about 80 meters. Figure 11 shows the concentration spatial distribution of H^+ after one year of mining. The migration amplitude of H^+ concentration is not as large as SO_4^{2-}.This may be due to H^+ being chemically active, which participates in more reactions and increases consumption during the migration process.

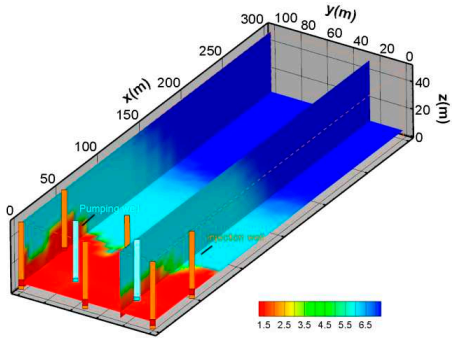

Figure 10. The spatial distribution of pH.

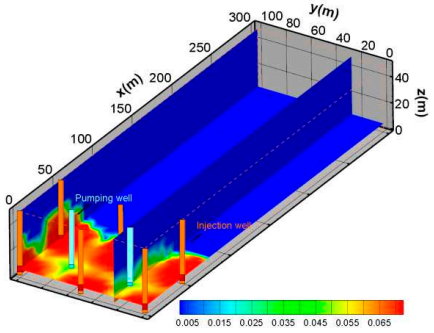

Figure 11. The spatial distribution of H^+.

 doi:10.20944/preprints202310.1980.v1

5.2. The pollution control results based on the water table

The analysis focuses first on the water table changes from scheme 1 to scheme 5 after mining for one year (Fig.12). Because the head near the injection well was elevated, the water table contours appeared convex. In addition, due to the head near the pumping well being reduced, the water table contours appeared groundwater depression cone. Figure 12a shows the head spatial distribution for the pumping ratio is 0 and the non-uniform injection ratio is 0. At the outside of the mining unit, the water level far from the mining area is not higher than the water level near the mining area. Figure 12b displays the head spatial distribution for the pumping ratio is 0.01 and the non-uniform injection ratio is 0. Due to the pumping ratio was not large enough, the water level is similar to scheme 1. Figure 12c shows the water table for the pumping ratio is 0.02 and the non-uniform injection ratio is 0. With the increase in pumping ratio, the groundwater depression cone is strengthened, and the water table convex is weakened. At the same time, in the outer area of the mining area, the water level far away from the mining area is higher than the water level near the mining area. Such water level features can prevent pollutants from migrating outside of the mining area. Figure 12d shows the water table for the pumping ratio is 0 and the non-uniform injection ratio is 0.05. With the increase in the non-uniform injection ratio, the cone of groundwater influence is strengthened, and the water table convex at the injection wells Q_4, Q_5, and Q_6 is weakened. In the outer area of the mining area, the water level far away from the mining area is higher than the water level near the mining area. Similarly, in the outer region of the mining area, the water level far from the mining area is higher than the water level near the mining area. Figure 12e represents the water table for the pumping ratio is 0 and the non-uniform injection ratio is 0.1. Under this condition, the water table convex at the injection wells Q_4, Q_5, and Q_6 is weakened more significantly. The groundwater depression cone can go through the gap between Q_4, Q_5, and Q_6, and develop to the outside of the mining area. In the outer region of the mining area, the water level far from the mining area is higher than the water level near the mining area. This characteristic is stronger than the scheme where the pumping ratio is 0.02 and the non-uniform injection ratio is 0.

Through the comparison of scheme 1, scheme 2, and scheme 3, the water table convex near the outer injection well is weakened with the increase of the pumping ratio. The water table out of the mining area shows the characteristics of high outside and low inside. That means with the increasing of the pumping ratio, the hydrodynamic field is more conducive to preventing pollution migration.

Through the comparison of scheme 1, scheme 4 and scheme 5 know that adopting non-uniform extraction, can achieve the same effect as the increase of the pumping ratio. When increasing the non-uniform injection ratio, under the same pumping ratio, the water table out of the mining area also displays the characteristics of high outside and low inside gradually. Therefore, the hydrodynamic field formed by increasing the non-uniform injection ratio is also beneficial to preventing pollution migration. For the non-uniform injection ratio is 0.05(scheme 4), this characteristic is weaker than the scheme where the pumping ratio is 0.02(scheme 3). For the non-uniform injection ratio is 0.1(scheme 5), this characteristic is stronger than the scheme where the pumping ratio is 0.02(scheme 3). Hence, increasing the non-uniform injection ratio can prevent the migration of pollutants more effectively.

Preprints (www.preprints.org) | NOT PEER-REVIEWED | Posted: 31 October 2023 doi:10.20944/preprints202310.1980.v1

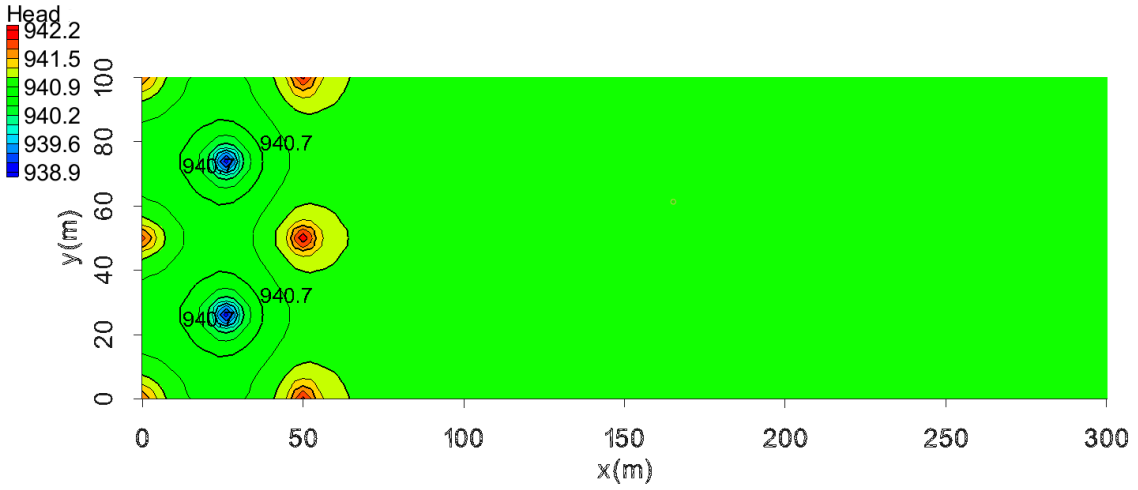

a. Water table map of scheme 1

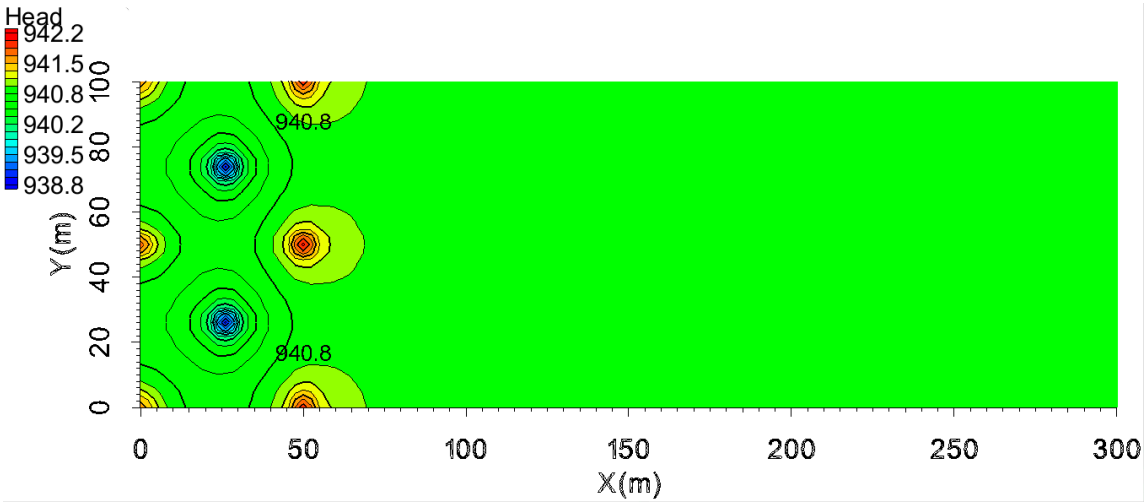

b. Water table map of scheme 2

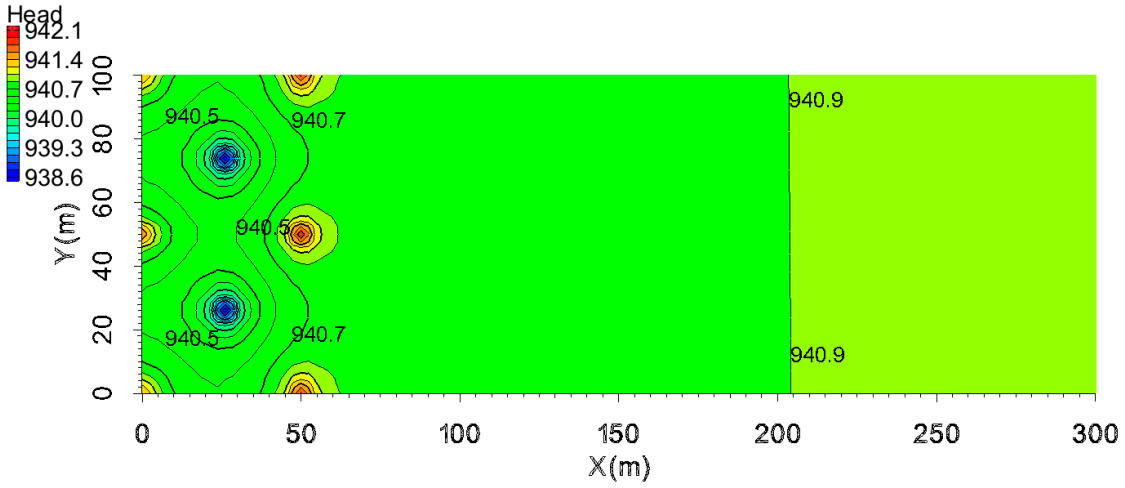

c. Water table map of scheme 3

Preprints (www.preprints.org) | NOT PEER-REVIEWED | Posted: 31 October 2023 doi:10.20944/preprints202310.1980.v1

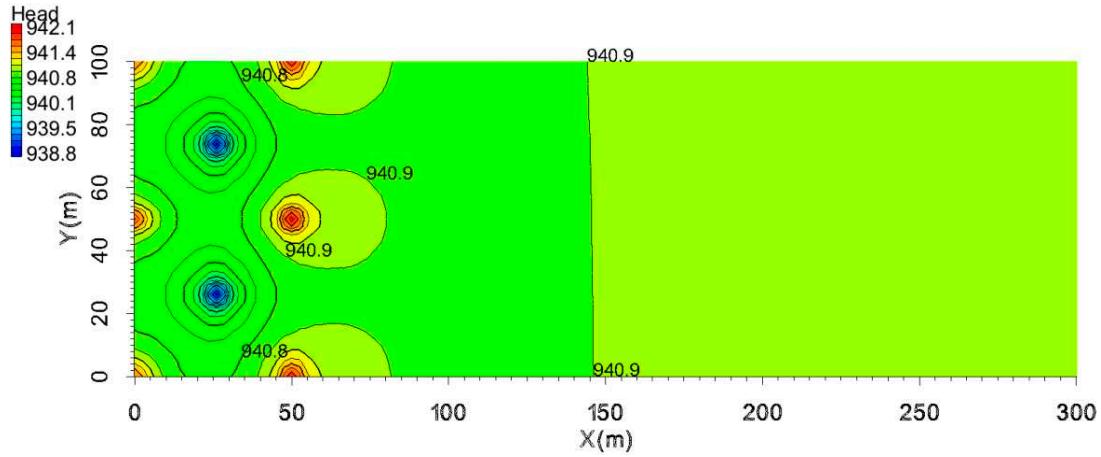

d. Water table map of scheme 4

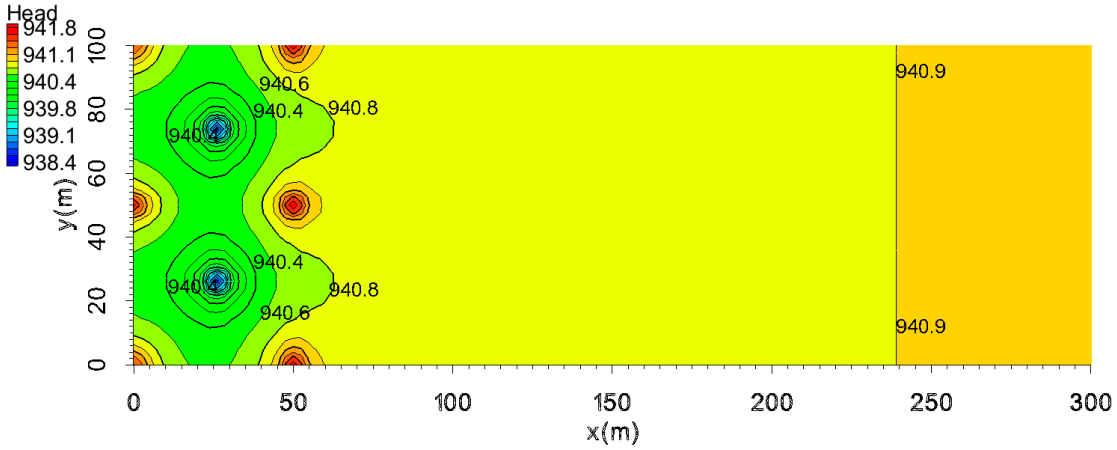

e. Water table map of scheme 5

Figure 12. Water table contour map of scheme1 to scheme 5(time=1year).

5.3. The hydrodynamic pollution control results based on streamline closure

Figure 13 represents the streamline closure of scheme 1 to scheme 5 after mining for one year (Fig.13). Figure 13a is the vertical cross section of the streamlines for the pumping ratio is 0 and the non-uniform injection ratio is 0 (Scheme 1). It revealed that this scheme formed a capture zone at a distance of approximately 130 meters as production continued. The envelope of the streamline extends gradually from the bottom to the upper slope. The blue line is the envelope of the streamline. As can be seen from the shape of the capture zone, a part of the streamline will bypass the envelope from the bottom to the periphery. This indicates that under the current flow conditions, there will be a part of the fluid that cannot be captured.

Figure 13b is the vertical cross section of the streamlines for the pumping ratio is 0.01 and the non-uniform injection ratio is 0 (scheme 2). The envelope shape of the streamline was changed. As can be seen from the figure, the envelope of the streamline points from 80 meters of the top plate to 150 meters of the bottom plate. At the same time, because the pumping is greater than the injection, the flow lines within the envelope are closed, and the flow lines outside the envelope show a tendency to converge inward.

Figure 13c provided the streamline and its envelope for the pumping ratio is 0.02 and the non-uniform injection ratio is 0 (scheme 3). The envelope of the streamline from 100 meters of the bottom plate to the pumping well. Compared with the scheme of Scheme2 (pumping ratio is 0.01), the envelope range is somewhat constricted.

Figure 13d shows the streamline and its envelope for the pumping ratio is 0 and the non-uniform injection ratio is 0.05 (scheme 4). The envelope of the streamline from 65m of the top plate to 115m of

Preprints (www.preprints.org) | NOT PEER-REVIEWED | Posted: 31 October 2023 doi:10.20944/preprints202310.1980.v1

the bottom plate. Because the pumping is greater than the injection, the flow lines within the envelope show a tendency to close, and the flow lines outside the envelope show a tendency to converge inward. Compared with the scheme of pumping ratio is 0.01, the envelope range is constricted. Respectively, the envelope of the streamline is looser than scheme3.

Figure 13e shows the streamline and its envelope for the pumping ratio is 0 and the non-uniform injection ratio is 0.1 (scheme 5). From the streamline characteristics of Fig 6e, the envelope range of the streamline is closer to the mining area. The maximum distance from the inner boundary to the envelope is less than 75 meters. The flow lines within the envelope are closed, and the flow lines outside the envelope show a tendency to converge inward. Compared with the other schemes, the envelope range is the most constricted.

By comparing the streamline characteristics of scheme 1, scheme 2, and scheme 3, it is found that the envelope of scheme 3 is closer to the mining area than scheme 1 and scheme 2. This indicated that its hydraulic capture is more effective. Therefore, scheme 3 with the pumping ratio is 0.02 is beneficial to preventing pollution migration. By comparing the streamline characteristics of scheme 1, scheme 4, and scheme 5, the result reveals that the best hydraulic capture occurred in scheme 5. Furthermore, the hydraulic capture effect is stronger than scheme 3. Hence, the best scheme for preventing pollution migration is the scheme5 with a pumping ratio is 0 and a non-uniform injection ratio is 0.1.

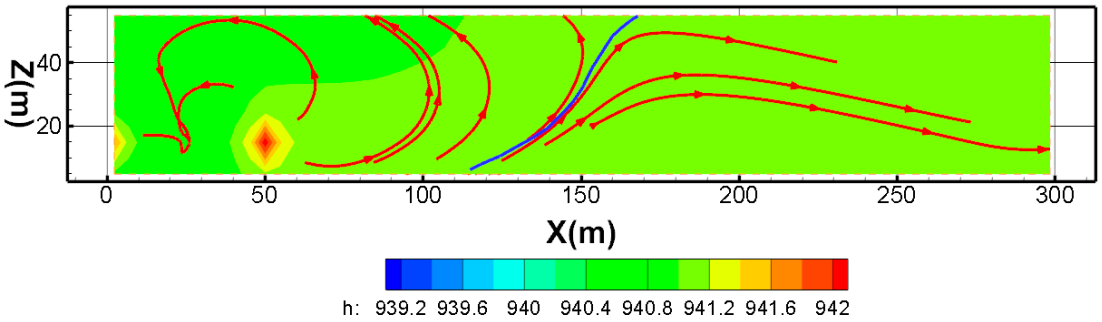

a. The vertical profile for the streamlines of scheme 1

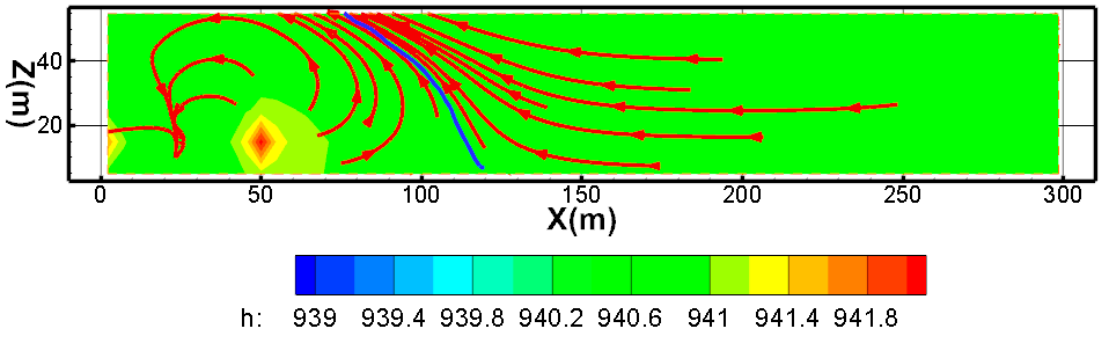

b. The vertical profile for the streamlines of scheme 2

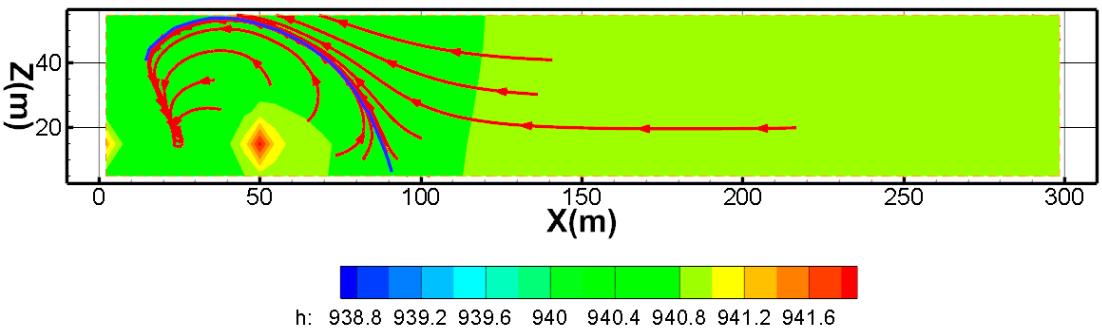

c. The vertical profile for the streamlines of scheme 3

Preprints (www.preprints.org) | NOT PEER-REVIEWED | Posted: 31 October 2023 doi:10.20944/preprints202310.1980.v1

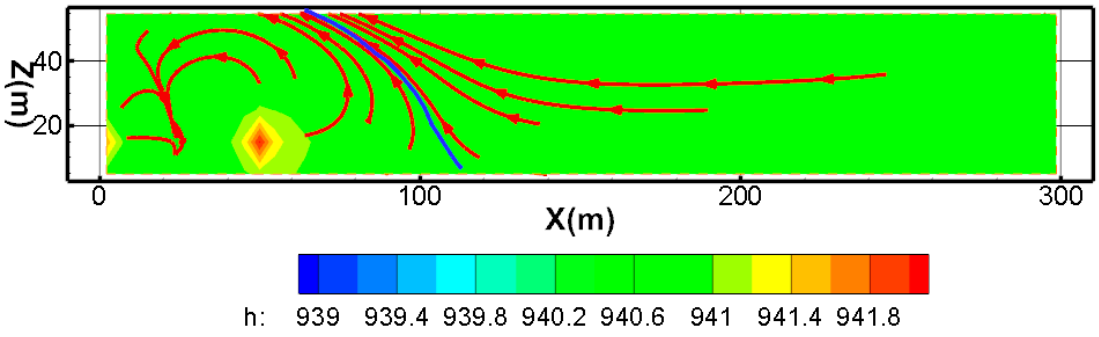

d. The vertical profile for the streamlines of scheme 4

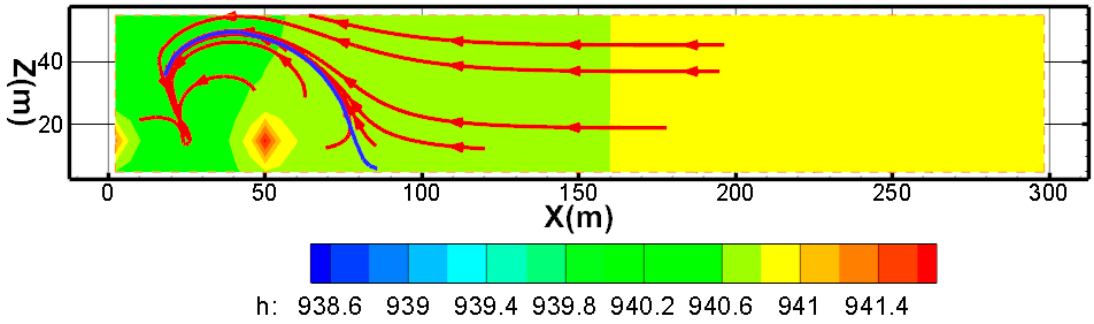

e. The vertical profile for the streamlines of scheme 5

Figure 13. The vertical profile for the streamlines of scheme 1 to scheme 5(time=1 year).

5.4. The pollution control results of concentration characteristics at well W_1 by RTM.

Combined with the above streamline characteristics, the grid of W_1 was selected as an observation point to extract the concentration of each index at this grid. Since the injected solution in the mining area contains sulfuric acid, pH and SO_4^{2-} are selected as two important single-factor indexes, while UO_2^{2+} is the radioactive nuclide index of groundwater. Meanwhile, there is a high risk for health, therefore, it is also an important single index. Therefore, the single-factor index focuses on UO_2^{2+}, SO_4^{2-}, and pH.

Figure 14 shows the variation of the concentrations of UO_2^{2+}, SO_4^{2-}, and H^+ at W_1. It can be seen in Fig. 13 that scheme 5 has the lowest concentration in different mining scenarios. This result suggests that adding the flow rate of the internal injection well (Q_1, Q_2, Q_3) and reducing the flow rate external injection well (Q_4, Q_5, Q_6) can effectively weaken the impact of ISL on the water environment in the surrounding area. The low concentration concentrations of UO_2^{2+}, SO_4^{2-}, and H^+ in scheme 3 suggest that raising the pumping ratio may also have a similar effect. As the pumping ratio increases, more non-ore groundwater will be extracted. In contrast, the effect of scheme 5 is more significant. This approach is a better choice because it has less of an impact on productivity.

Preprints (www.preprints.org) | NOT PEER-REVIEWED | Posted: 31 October 2023 doi:10.20944/preprints202310.1980.v1

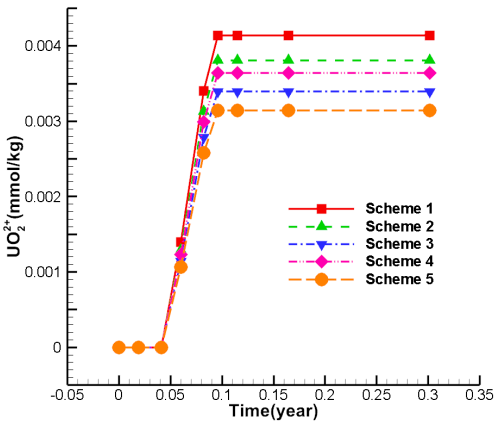

a. The concentration variation of UO_2^{2+}

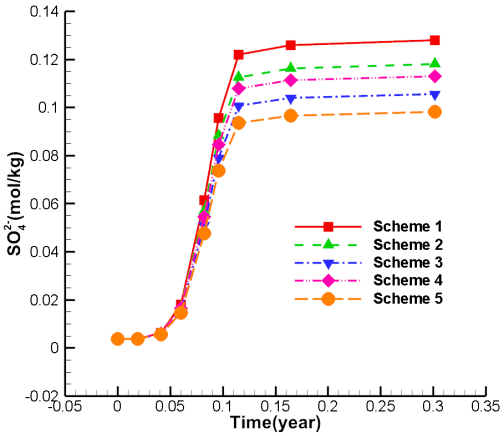

b. The concentration variation of SO_4^{2-}

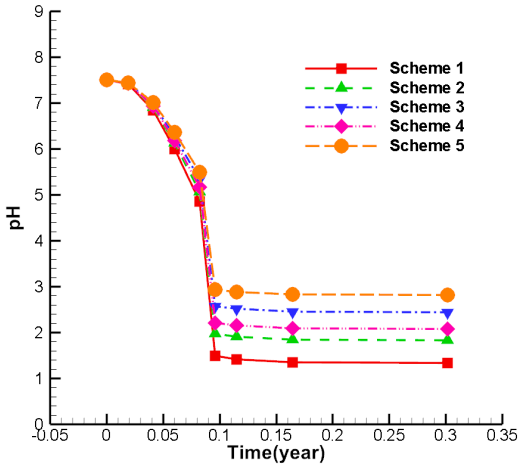

c. The value variation of pH

Figure 14. Variation of UO_2^{2+}, SO_4^{2-}, and pH of different pumping ratio and non-uniform injection ratio in the selected grid W_1.

5.5. The sensitivity analysis of the influence of pumping ratio and non-uniform injection ratio

In order to better understand the influence of pumping ratio and non-uniform injection ratio, a sensitivity analysis was performed for them. The pumping ratio is between 0 to 0.05, the non-uniform injection ratio is between 0 to 1. According to the formation(18) and formation(19), the sensitivity is calculated by:

$$S_i = \frac{C_i - C_1}{\xi_i - \xi_1} \tag{20}$$

Where i represents the scheme number, C_i represents the concentration of scheme i at well W_1, the ξ_i represents the pumping ratio and non-uniform injection ratio of scheme i. S_i is the sensitivity of scheme i.

Preprints (www.preprints.org) | NOT PEER-REVIEWED | Posted: 31 October 2023 doi:10.20944/preprints202310.1980.v1

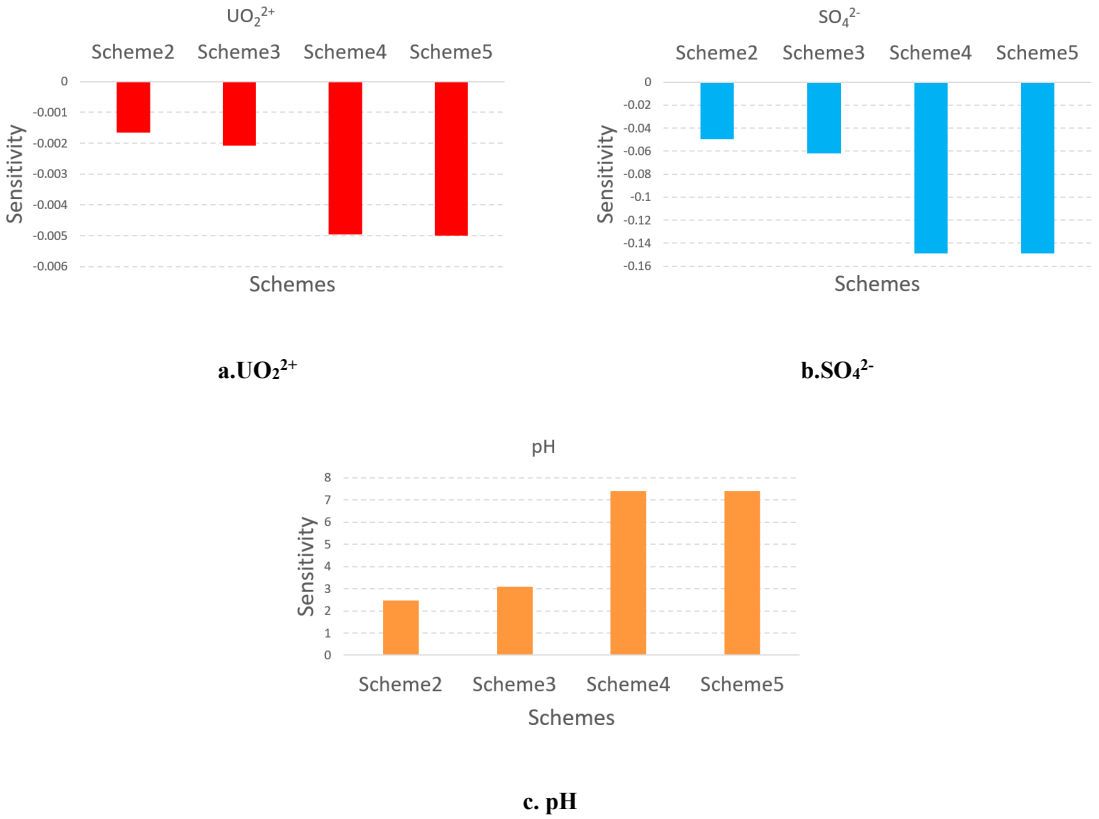

a.UO_2^{2+} **b.SO_4^{2-}**

c. pH

Figure 15. The sensitivity coefficient of different pumping ratios and non-uniform injection ratio on the concentration of UO_2^{2+}, SO_4^{2-}, pH.

Through the sensitivity analysis of the above five schemes, it can be seen in Fig. 8 that the influence of the non-uniform injection scheme on the concentration of the three ions is greater than the increasing pumping ratio. This indicates that the non-uniform injection scheme has a more significant impact on pollution control. At the same time, Scheme 5 is a better choice because the concentration of UO_2^{2+}, SO_4^{2-}, and H^+ at W_1 in this scheme is the lowest. Therefore, the beneficial impact is strongest. In this scheme, the non-uniform injection ratio is 0.1. The inner injection rate is 194.09m^3/d, the outer injection rate is 158.89m^3/d, and the pumping rate is 264.00m^3/d.

6. Conclusions

In this study, the reactive transport simulation in the process of ISL is carried out by selecting an extended strip area at the edge of the mining area in Bayan-Uul. The model depicts the migration distance and changes trend of UO_2^{2+}, H^+, SO_4^{2-}, and other hydrochemical components that are involved in mining. From the model, we can infer that the water level, the streamlines, the capture zone, and the concentration of UO_2^{2+}, H^+, SO_4^{2-} at W_1 well. Several schemes controlled by pumping ratio, and non-uniform injection ratio, were simulated and compared.

The simulation results reveal that the greater the pumping ratio and non-uniform injection ratio are, the closer the migration distance of the groundwater pollution in the mining area is. When the pumping ratio increases gradually, a capture zone will be formed near the mining area. The hydraulic capture effect of the capture zone on groundwater will be more pronounced and advantageous in preventing the outward migration of groundwater contamination the higher the pumping ratio. When the flow rate of the internal injection well increases and the flow rate of the marginal injection well is reduced, the capture zone will also be formed near the mining area. Through the comparison of pumping ratio and non-uniform injection ratio, the results show that non-uniform injection ratio equal 0.1 is the most beneficial to format the hydraulic capture zone. In this scheme, the inner injection rate is 194.09m^3/d, the outer injection rate is 158.89m^3/d, and the pumping rate is 264.00m^3/d. Based

on the sensitivity analysis of pumping ratio, and non-uniform injection ratio, the non-uniform pumping mode (Scheme 5) is more effective than the scheme that simply increases the pumping ratio. The analysis of ion concentration in different mining conditions shows that the non-uniform pumping mode can improve the influence of acid-leaching on groundwater quality.

In summary, it is suggested to combine the non-uniform mining mode in the process of uranium leaching. In this way, the pollution of the groundwater environment caused by in-situ uranium leaching can be controlled better.

Funding: The financial support of this work reported here is provided by the Joint fund key support project NSFC (u1911205). The field survey work is supported by project A60-3 of the Chemical Metallurgy Research Institute.

Acknowledgments: This study was completed under the guidance of Prof. Zhonghua Tang from the China University of Geosciences(Wuhan). The work is supported partially by the Beijing Research Institute of Chemical Engineering and Metallurgy. The authors would like to thank Prof. Jili Wen from the Beijing Research Institute of Chemical Engineering and Metallurgy for advising the work. Editors and anonymous reviewers are also thanked for their valuable comments in improving the quality of the manuscript.

References

1. Saunders: J.A.; Pivetz, B.E.; Voorhies, N.; Wilkin, R.T. Potential aquifer vulnerability in regions down-gradient from uranium in situ recovery (ISR) sites. *J Environ Manage* **2016**, *183*, 67-83.
2. Bhargava, S.K.; Ram, R.; Pownceby, M.; Grocott, S.; Ring, B.; Tardio, J.; Jones, L. A review of acid leaching of uraninite. *Hydrometallurgy* **2015**, *151*, 10-24.
3. Wellmer, F.W.; Becker-Platen, J.D. Sustainable development and the exploitation of mineral and energy resources: a review. *International Journal of Earth Sciences* **2002**, *91*, 723-745.
4. Poole, T.; Bruneton, P.; Fairclough, M.; Schnell, H.; Valter, O. Uranium Resources as Co- and By-products of Polymetallic Base, Rare Earth and Precious Metal Ore Deposits; *International Atomic Energy Agency*: **2018**.
5. Tulsidas, H.; Fairclough, M. *World Distribution of Uranium Deposits (UDEPO)*. **2018**.
6. Edwards, C.R.; Oliver, A.J. Uranium processing: A review of current methods and technology. *JOM: the journal of the Minerals, Metals & Materials Society* **2000**, *52*, 12-20.
7. Mudd, G.M. Critical review of acid in situ leach uranium mining: 2. Soviet Block and Asia. *Environ. Geol.* **2001**, *41*, 404-416.
8. Zhang, C.; Tan, K.; Xie, T.; Tan, Y.; Kong, L.J.P. Flow Microbalance Simulation of Pumping and Injection Unit in In Situ Leaching Uranium Mining Area. *Processes* **2021**, *9*, 1288.
9. Zhang, C.; Xie, T.T.; Tan, K.X.; Yao, Y.X.; Wang, Y.A.; Li, C.G.; Li, Y.M.; Zhang, Y.; Wang, H. Hydrodynamic Simulation of the Influence of Injection Flowrate Regulation on In-Situ Leaching Range. *Minerals* **2022**, 12, 15.
10. Collet, A.; Regnault, O.; Ozhogin, A.; Imantayeva, A.; Garnier, L. Three-dimensional reactive transport simulation of Uranium in situ recovery: Large-scale well field applications in Shu Saryssu Bassin, Tortkuduk deposit (Kazakhstan). *Hydrometallurgy* **2022**, *211*, 105873.
11. Mibus, J.; Sachs, S.; Pfingsten, W.; Nebelung, C.; Bernhard, G. Migration of uranium(IV)/(VI) in the presence of humic acids in quartz sand: a laboratory column study. *J Contam Hydrol* **2007**, 89, 199-217.
12. Kurmanseiit, M.B.; Tungatarova, M.S.; Kaltayev, A.; Royer, J.J. Reactive Transport Modeling during Uranium In Situ Leaching (ISL): The Effects of Ore Composition on Mining Recovery. *Minerals* **2022**, *12*, 21.
13. Yabusaki, S.B.; Fang, Y.; Waichler, S.R. Building conceptual models of field-scale uranium reactive transport in a dynamic vadose zone-aquifer-river system. *Water Resources Research* **2008**, 44.
14. Kohler, M.; Curtis, G.P.; Kent, D.B.; Davis, J.A. Experimental Investigation and Modeling of Uranium (VI) Transport Under Variable Chemical Conditions. *Water Resources Research* **1996**, 32, 3539-3551.
15. Zhang, X.; Jiao, C.; Wang, J.; Liu, Q.; Li, R.; Yang, P.; Zhang, M. Removal of uranium(VI) from aqueous solutions by magnetic Schiff base: Kinetic and thermodynamic investigation. *Chemical Engineering Journal* **2012**, 198-199, 412-419.
16. 12. Bear, J.; Jacobs, M. On the movement of water bodies injected into aquifers. *Journal of Hydrology* **1965**, *3*, 37-57.
17. 13. Xu Shaohui, Z.X. Hydraulic interception technology and numerical simulation of groundwater oil pollution control. *JOUR NAL OF HYDRAULIC ENGINEERING* **1999**, 71-76.
18. 14. Javandel, I.; Tsang, C.F. Capture-zone type curves-A tool for aquifer cleanup. *Ground Water* **1986**, *24*, 616-625.
19. Faybishenko, B.A.; Javandel, I.; Witherspoon, P.A. Hydrodynamics of the capture zone of a partially penetrating well in a confied aquifer. *Water Resources Research* **1995**, *31*, 859-866.

20. Bair, E.S.; Roadcap, G.S. Comparison of flow models used to delineate capture zones of wells.1.leaky-confined fractured-car bonate aquifer. *Ground Water* **1992**, *30*, 199-211.
21. Wang, J.C.; Booker, J.R.; Carter, J.P. Analysis of the remediation of a contaminated aquifer by a multi-well system. *Computers and Geotechnics* **1999**, *25*, 171-189.
22. Hudak, P.F. Numerical modeling assessment of three-gate structures for capturing contaminated groundwater. *Environ. Geol.* **2008**, *55*, 1311-1317.
23. Zheng, H.Q.Y. Site conditions experiments for field test on in-situ leaching and hydrodynamic simulation of uranium in Bayan-Uul. University of Technology(Nanchang),East China. **2017**.
24. Chang, Y. Simulation study on groundwater dynamics control of leaching range of in-situ uranium well field. University of South China **2020**.
25. Chen, Q.Q. Numerical Simulation of In-situ Leaching of Uranium by Acid Method Based on Reactive Solute Transport Theory. University of Technology(Nanchang),East China. **2020**.
26. Xu, T.; Spycher, N.; Sonnenthal, E.; Zheng, L.; Pruess, K. TOUGHREACT_V2_Users_Guide. **2012**.
27. Xu, T.; Apps, J.A.; Pruess, K. Reactive geochemical transport simulation to study mineral trapping for CO2 disposal in deep arenaceous formations. *Journal of Geophysical Research: Solid Earth* **2003**, 108.
28. Pruess, K.; Oldenburg, C.M.; Moridis, G.J. TOUGH2 User's Guide Version 2. United States: N. p. Web. **1999**.
29. Xu, T.; Spycher, N.; Sonnenthal, E.; Zhang, G.; Zheng, L.; Pruess, K. TOUGHREACT Version 2.0: A simulator for subsurface reactive transport under non-isothermal multiphase flow conditions. *Computers geosciences* **2011**, *37*, 763-774.
30. Dobson, P.F.; Salah, S.; Spycher, N.; Sonnenthal, E.L. Simulation of water-rock interaction in the yellowstone geothermal system using TOUGHREACT. *Geothermics* **2004**, *33*, 493-502.
31. Sonnenthal, E.; Ito, A.; Spycher, N.; Yui, M.; Apps, J.; Sugita, Y.; Conrad, M.; Kawakami, S. Approaches to modeling coupled thermal, hydrological, and chemical processes in the drift scale heater test at Yucca Mountain. *International Journal of Rock Mechanics and Mining Sciences* **2005**, *42*, 698-719.
32. Spycher, N.F.; Sonnenthal, E.L.; Apps, J.A. Fluid flow and reactive transport around potential nuclear waste emplacement tunnels at Yucca Mountain, Nevada. *J Contam Hydrol* **2003**, *62-63*, 653-673.
33. Aradottir, E.S.P.; Sonnenthal, E.L.; Bjornsson, G.; Jonsson, H. Multidimensional reactive transport modeling of CO2 mineral sequestration in basalts at the Hellisheidi geothermal field, Iceland. *International Journal of Greenhouse Gas Control* **2012**, *9*, 24-40.
34. Audigane, P.; Gaus, I.; Czernichowski-Lauriol, I.; Pruess, K.; Xu, T.F. Two-dimensional reactive transport modeling of CO2 injection in a saline Aquifer at the Sleipner site, North Sea. *Am. J. Sci.* **2007**, *307*, 974-1008.
35. Zheng, C.M.; Bennett, G.D. Applied Contaminant Transport Modeling(Second Edition); **2002**.